# Development of a bioresorbable self-expanding microstent for interventional applications – an innovative approach for stent-assisted coiling

## Entwicklung eines bioresorbierbaren, selbstexpandierenden Mikrostents für interventionelle Anwendungen – ein innovativer Ansatz für stentgestütztes Coiling

Authors

Hagen Paetow[1], Felix Streckenbach[2], Christoph Brandt-Wunderlich[1], Wolfram Schmidt[3], Michael Stiehm[1], Sönke Langner[2], Daniel Cantré[2], Marc-André Weber[2], Klaus-Peter Schmitz[1, 3], Stefan Siewert[1]

Affiliations

1 Institute for Implant Technology and Biomaterials e.V., Rostock, Germany
2 Institute of Diagnostic and Interventional Radiology, Pediatric Radiology and Neuroradiology, Rostock University Medical Center, Rostock, Germany
3 Institute for Biomedical Engineering, Rostock University Medical Center, Rostock, Germany

Key words

self-expanding stent, neurovascular, performance testing, bioresorbable

**received** 1.3.2023
**accepted** 9.11.2023
**published online** 13.12.2023

Bibliography

Fortschr Röntgenstr 2024; 196: 714–725
**DOI** 10.1055/a-2211-2983
**ISSN** 1438-9029

Georg Thieme Verlag KG, Rüdigerstraße 14, 70469 Stuttgart, Germany

Correspondence

Dr. Stefan Siewert
Institute for Implant Technology and Biomaterials e.V., Friedrich-Barnewitz-Straße 4, 18119 Rostock-Warnemünde, Germany
Tel.: +49/3 81/54 34 56 03
stefan.siewert@iib-ev.de

ABSTRACT

**Objectives** Stent-assisted coiling prevents coil migration in broad-based intracranial aneurysms. So far, only permanent metal stents are approved for intracranial use. Bioresorbable stents allow a new therapeutic approach that may prevent the need for lifelong anticoagulation. We developed a neurovascular bioresorbable microstent (NBRS) and compared it *in vitro* to the commercial Neuroform EZ stent.

**Materials and Methods** The self-expanding NBRS design is oriented on the Neuroform EZ stent. Poly L-lactic acid (PLLA) was used to manufacture semi-finished products in a dipping process. For the compensation of the inferior material properties of PLLA, design adjustments were made. The NBRS were cut by means of femtosecond (fs) laser and were morphologically and mechanically compared *in vitro* to the Neuroform EZ stent. *In vitro* implantation of an NBRS was performed using a complex patient-specific 3D-printed aneurysm model. In addition, an *in vitro* coiling procedure to assess the stent's ability to support a coil package was conducted.

**Results** The NBRS could be reproducibly manufactured and had high quality regarding surface morphology. The radial force at the indicated vessel diameter of 3.0 mm was slightly higher for the Neuroform EZ stent compared to the NBRS. The self-expansion ability of the NBRS could be proven. The kink behavior of the NBRS was comparable to that of the Neuroform EZ stent, so no vessel lumen size reduction is expected. The stents showed identical deformation under local compression of 25 % based on the initial diameter, resulting in maximum forces of 24 ± 5 mN (Neuroform EZ) and 8 ± 2 mN (NBRS). The implanted NBRS expanded uniformly, and proper vessel wall adaptation was observed. The NBRS has the ability to retain a coil package.

**Conclusion** This study reported a reproducible manufacturing process for the developed NBRS as well as mechanical and morphological *in vitro* tests. Furthermore, successful NBRS implantation into a complex patient-specific vessel model was presented as proof of concept. The promising results of this study, also considering the commercial Neuroform EZ stent, support the idea of fully biodegradable microstents for intracranial aneurysm treatment.

### Key Points

- High-performance polymer-based self-expanding neurovascular microstents were manufactured with good reproducibility.
- The bioresorbable microstent meets the requirements to pass through narrow radii.

- Implantability in a patient-specific and close-to-physiology vascular *in vitro* model was proven.

**Citation Format**

- Paetow H, Streckenbach F, Brandt-Wunderlich C et al. Development of a bioresorbable self-expanding microstent for interventional applications – an innovative approach for stent-assisted coiling. Fortschr Röntgenstr 2024; 196: 714–725

## ZUSAMMENFASSUNG

**Ziel** Stent-gestütztes Coiling verhindert die Coilmigration bei breitbasigen, intrakraniellen Aneurysmen. Bislang sind nur permanente Metallstents für intrakranielle Anwendungen zugelassen. Bioresorbierbare Stents ermöglichen einen neuen therapeutischen Ansatz, bei dem die Notwendigkeit einer lebenslangen Antikoagulation vermieden werden könnte. Wir haben einen neurovaskulären bioresorbierbaren Mikrostent (NBRS) entwickelt und *in vitro* mit dem kommerziellen Neuroform EZ-Stent verglichen.

**Material und Methoden** Das mit computergestützter Design-Software erstellte selbstexpandierende NBRS-Design orientiert sich am Neuroform EZ. Zum Ausgleich unterlegener Materialeigenschaften wurden Designanpassungen vorgenommen. Poly L-Milchsäure (PLLA) wurde zur Herstellung von Halbzeugen im Tauchverfahren verwendet. Die NBRS wurden mittels Femtosekunden (fs)-Laser geschnitten. Darauf aufbauend erfolgten *in vitro* morphologische und mechanische Untersuchungen sowie ein Benchmark mit dem Neuroform EZ. Eine *in vitro* Implantation eines NBRS unter Verwendung eines komplexen patientenspezifischen 3D-gedruckten Aneurysma-Modells sowie eine *in vitro* Coiling-Prozedur zur Bewertung der Rückhaltefähigkeit des NBRS wurden durchgeführt.

**Ergebnisse** Die NBRS konnten reproduzierbar und qualitativ hochwertig hergestellt werden. Der Neuroform EZ zeigte bei einem Einsatzdurchmesser von 3,0 mm eine leicht höhere Radialkraft als der NBRS. Die Selbstaufweitfähigkeit des NBRS wurde nachgewiesen. Das Knickverhalten des NBRS war vergleichbar mit dem Neuroform EZ, sodass keine Reduktion des Gefäßlumens zu erwarten ist. Die Stents zeigten eine identische Verformung unter 25 % lokaler Kompression, bezogen auf den ursprünglichen Durchmesser, was zu maximalen Kräften von 24 ± 5 mN (Neuroform EZ) und 8 ± 2 mN (NBRS) führte. Die Expansion des implantierten NBRS erfolgte gleichmäßig und es wurde eine vollständige Anpassung an die Gefäßwand beobachtet. Die Fähigkeit des NBRS, ein Coil-Paket zurückzuhalten, konnte bestätigt werden.

**Schlussfolgerung** Diese Studie berichtet über einen reproduzierbaren Herstellungsprozess für die entwickelten NBRS sowie mechanische und morphologische *in vitro* Tests. Darüber hinaus wurde eine erfolgreiche NBRS-Implantation in ein komplexes patientenspezifisches Gefäßmodell als Konzeptnachweis vorgestellt. Die vielversprechenden Ergebnisse dieser Studie, unter Berücksichtigung des kommerziellen Neuroform EZ-Stents, stützen die Idee vollständig bioresorbierbarer Mikrostents für die Behandlung intrakranieller Aneurysmen.

**Kernaussagen**

- Leistungsfähige polymerbasierte, selbstexpandierende, neurovaskuläre Mikrostents konnten reproduzierbar hergestellt werden.
- Der resorbierbare Mikrostent erfüllt die Anforderungen, enge Radien zu passieren.
- Die Implantatierbarkeit in einem patientenspezifischen und physiologienahen *in vitro* Gefäßmodell wurde nachgewiesen.

## Introduction

Stent-assisted endovascular coil embolization of an intracranial aneurysm is an established interventional procedure, allowing treatment of complex and challenging broad-necked aneurysms, by preventing coil protrusion or dislocation of coils into the parent artery [1, 2]. Thrombosis in the aneurysm and an inflammatory reaction in the surrounding tissue occlude and stabilize the aneurysm, followed by formation of endothelial layer at the aneurysm neck [3].

Cho et al. investigated the physical properties of four commercial self-expanding intracranial stents, showing that the Neuroform EZ stent was generally in the midrange, but achieves above-average to excellent results regarding radial force and surface roughness [4]. The open cell Nitinol stent with four radiopaque markers at the proximal and distal end can access aneurysms in tortuous vascular passages [5].

Due to the implanted foreign material, inhibition of platelet aggregation is usually performed as a dual therapy during the first year after implantation, followed by lifelong administration of acetylsalicylic acid (ASA). However, there is still insufficient long-term experience with regard to implanted intracranial stents [6].

Bioresorbable stents (BRS) made of metals or polymers, particularly magnesium alloys and poly L-lactic acid (PLLA) offer a new therapeutic approach in the treatment of intracranial aneurysms as well as stenoses and are part of current studies and reviews [7]. In contrast to conventional metallic stents, BRS dissolve after a certain time and are metabolized by the body [8]. Platelet inhibition might be avoidable after the BRS dissolves, thus decreasing the risk of hemorrhagic complications [9, 10]. Finally, nonmetal BRS have fewer artifacts on computed tomography (CT) and magnetic resonance imaging (MRI), thus facilitating follow-up imaging. However, these BRS are generally of low radiopacity needing radiopaque markers for X-ray visibility [11].

The aim of the current study was to design, manufacture, and examine a neurovascular bioresorbable microstent (NBRS) prototype based on a commercially available product suitable to treat broad-based intracranial aneurysms.

Within this proof-of-concept study, an NBRS prototype was investigated regarding morphology and fundamental mechanical properties. Furthermore, simulated use tests including implantation of the device into a 3D-printed patient-specific phantom model under physiological-orientated conditions and an *in vitro*

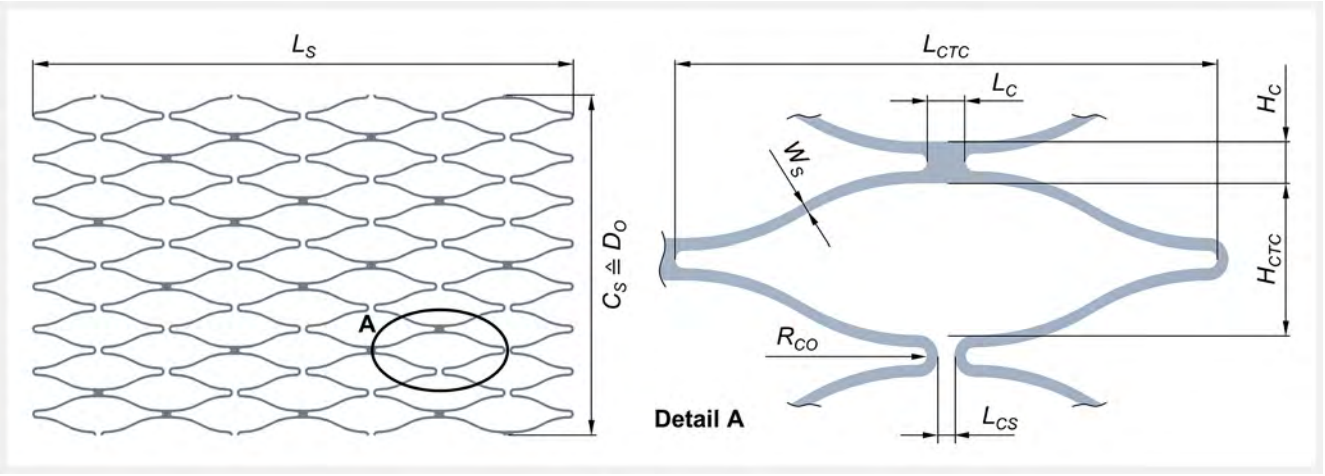


▶ **Fig. 1** Design of bioresorbable self-expanding microstent: stent length ($L_S$), stent circumference ($C_S$) or stent outer diameter ($D_O$), cell-to-cell length ($L_{CTC}$), cell-to-cell height ($H_{CTC}$), connector length ($L_C$), connector height ($H_C$), peak-to-peak cell spacing ($L_{CS}$), cell opening radius ($R_{CO}$), and strut width ($W_S$).

coiling procedure to assess the stent's ability to support a coil package were performed.

## Materials and Methods

### Design of a neurovascular bioresorbable microstent

In the current study, an NBRS design oriented on the Neuroform EZ stent (Stryker Corp., USA) was developed (see ▶ **Fig. 1**). This commercial device has a nominal outer diameter of $D_O = 3.5$ mm and length of $L_S = 20$ mm. This stent is approved to treat wide neck, intracranial, saccular aneurysms combined with the use of embolic coils and is recommended for a parent vessel size of 3.0 mm < $D_V \leq 3.5$ mm.

Since PLLA shows inferior mechanical properties compared with Nitinol, the NBRS wall thickness $T_W$ and strut width $W_S$ were increased to 100 µm to improve the mechanical properties of the NBRS prototype – particularly to enhance the bending stiffness, the radial stiffness, and the resistance to local deformation. An outer stent diameter of $D_O = 4.0$ mm in the fully expanded state was chosen, aiming for an indicated use in the parent vessels of $D_V = 3.0$ mm. To improve the overall stiffness of the NBRS structure, the connector elements between meander structures were increased in length as well as height to about $L_C = H_C = 360$ µm and cell spacing was reduced by about 55 µm. As a result, the described design changes led to a minimum crimping diameter of 1 mm. The stent design was implemented using Creo Parametric 6.0 software (Parametric Technology Corp., USA).

### Manufacturing of semi-finished products

Tubes as semi-finished products for the NBRS were manufactured based on a PLLA (Resomer L210 S, Evonik Health Care GmbH, Germany) in chloroform (Carl Roth GmbH + Co. KG, Germany) solution (3 g of PLLA dissolved in 100 ml chloroform) using a semi-automatic dipping process as described previously [12]. In short, stainless steel mandrels with a diameter of 4.0 mm and a length of 55 mm were used for repeated dipping into the polymer solution. This process was performed using a KSV NIMA Dip Coater (Biolin Scientific Holding AB, Sweden) at (22 ± 2) °C and 25 % humidity. After each repetition, the mandrels were dried for 10 minutes and turned over by 180°. After twelve cycles the desired wall thickness of 100 µm was achieved.

The tubing outer diameter was measured by means of a biaxial laser scanner (ODAC 32 XY, Zumbach Electronic AG, Switzerland) in 0.5 mm increments along the longitudinal axis. The tube wall thickness $T_W$ along the longitudinal axis was determined using the arithmetic mean of the outer tubing diameter $D_T$ and the outer mandrel diameter $D_M$ according to equation 1. Furthermore, the average wall thickness variation $T_{VAR}$ was calculated from the mean of the maximum $D_{Tmax}$ and minimum outer tube diameter $D_{Tmin}$ as well as the mean tube wall thickness according to equation 2.

$$T_W = \frac{D_T - D_M}{2} \quad (1)$$

$$T_{VAR} = \frac{(D_{Tmax} - D_{Tmin})}{2T_W} \quad (2)$$

The mandrels were removed and PLLA tubes were dried for 24 h at 40 °C. In order to minimize residual solvent content, the PLLA tubes were washed in methanol and deionized water using a platform-shaking device (Unimax 1010, Heidolph Instruments GmbH & Co. KG, Germany) at 100 rpm and 20 °C, for two days each. Finally, the PLLA tubes were dried for two days in a vacuum at 40 °C.

For NBRS fs-laser manufacturing, PLLA tubes with a minimum length of 21 mm and a maximum average wall thickness variation of $T_{VAR}$ = 20 % were selected.

## Femtosecond-laser manufacturing of microstents

NBRS manufacturing was conducted using an fs-laser system (Monaco 1035-80-60, Coherent Inc., USA) embedded into a 4-axis CNC system (Star Cut Tube Monaco, Coherent Munich GmbH & Co. KG, Germany). The NBRS design was transferred into a numerical control (NC) file using CAGILA (CAM-Service GmbH, Germany). PLLA tubes were mounted on a 4 mm ceramic mandrel and clamped in the laser system jaw chuck. Fs-laser processing was conducted at a pulse rate of 10 kHz, with a pulse width of 276 fs and power of 0.3 W at a cutting speed of 1 mm $s^{-1}$ using Argon at 0.5 bar as the process gas.

## Geometrical and morphological examination of microstents

Geometrical and morphological analyses were performed utilizing three NBRS prototypes and one Neuroform EZ. Macroscopic images of the NBRS as well as a Neuroform EZ stent were taken using a digital camera (EOS 70 D with Zoom Lens EF-S 18–55 mm 1:3.5–5.6 II, EF 55–200 mm 1:4.5–5.6 II USM, Canon, Japan) and reversal adapter (EOS-Retro, Novoflex, Germany).

Stent length measurements were performed with a micrometer gauge (No. 164-163, Mitutoyo, Japan). Further geometrical dimensions (▶ **Fig. 1**) were investigated by optical microscopy (SZX16 with UC30 camera, Olympus, Japan). For measuring the stent length at an intended vessel diameter, the stents were deployed into a transparent rigid tube with an inner diameter of 3.0 mm. Surface morphology and cutting edges were analyzed by means of scanning electron microscopy (SEM; Quattro S, Thermo Fisher Scientific, USA) in environmental scanning mode at 0.5 mbar and 15 kV. The vessel coverage ratio *VCR* was determined according to equation 3 comparing the mass of the stent with the mass of an ideal hollow cylinder with an appropriate wall thickness and density [13].

$$VCR = \frac{m_{stent}}{m_{hollow\ cylinder}} \cdot 100\ \% \qquad (3)$$

The mass was measured with a precision balance (Comparator XP6U, Mettler Toledo, Switzerland) and the density was estimated based on values from the literature (1.24 g/cm³ for PLLA; 6.40 g/cm³ for Nitinol) [14, 15].

## Radial force and radial stiffness

Investigation of the radial force behavior was performed with a segmented head testing machine (TTR2 with J-Crimp station, Blockwise Engineering LCC, USA) at 37 ± 2 °C and a velocity of 0.05 mm $s^{-1}$. Radial forces were measured from a fully expanded state down to a minimum diameter of 1.0 mm and evaluated at the intended vessel diameter of 3.0 mm during compression (radial resistive force, RRF) as well as during expansion (chronic outward force, COF). Additionally, the radial stiffness, represented by the initial increase of the radial force curve, was assessed. After radial force testing, the stent outer diameter $D_{O,C}$ was measured by optical microscopy at five positions along the longitudinal axis and compared to the nominal diameter $D_O$ in a fully expanded state prior to radial force testing (▶ **Fig. 2**).

### Kink behavior

The kink behavior was investigated by bending the stents around cylindrical mandrels with radii ranging from 32.5 mm to 7.5 mm in 2.5 mm steps and from 7.5 mm to 2.5 mm in 1.25 mm steps [16]. A 0.014" guide wire (Cruiser F, BIOTRONIK, Switzerland) was inserted into the stent and bent 180° around a mandrel to contact the stent and mandrel over the entire length. The bent state was documented using a digital camera (EOS 70 D, Zoom Lens EF-S 18–55 mm, Olympus, Japan). The analysis was conducted under ambient conditions at 21 ± 2 °C in air.

## Resistance to local deformation

During stent-assisted coiling, the stent is locally loaded in the radial direction. For measurement of radial resistance to local deformation, the expanded stent was deformed by a prismatic plunger with a 1 mm radius. The plunger was connected to a universal testing machine (Zwick BT1-FR2.5TN.D14, ZwickRoell GmbH & Co. KG, Germany) using a 20 N load cell (XForce HP, ZwickRoell GmbH & Co. KG, Germany).

The force distance curves were measured at 37 ± 2 °C in air using a cross head speed of 5 mm $min^{-1}$ until a maximum local reduction of stent diameter of 25 % was achieved.

## Simulated use and stent release *in vitro*

For analysis of NBRS applicability, a simulated use test setup combined with a patient-specific neurovascular vessel model was used (▶ **Fig. 3**), as described previously [17]. The test setup based on A. Kemmling's flow model consists of a water bath including the patient-specific vessel model connected to an 80 cm long arterial access vessel and a 6F introducer sheath (Terumo Radifocus Introducer II, Japan) [18]. A pulsatile pump (FlowTek 125, United Biologics Inc., USA) was connected to circulate water at 37 ± 2 °C, applying a flow rate of 1.4 l $min^{-1}$ at a pulse rate of 60 $min^{-1}$.

The vessel model was manufactured using a Form 2 3D printer and Clear Resin (Formlabs Inc., USA). The complex model curvature is illustrated in ▶ **Fig. 3** and was quantified by angles and radii. NBRS implantation was conducted using a straight 4F angio-

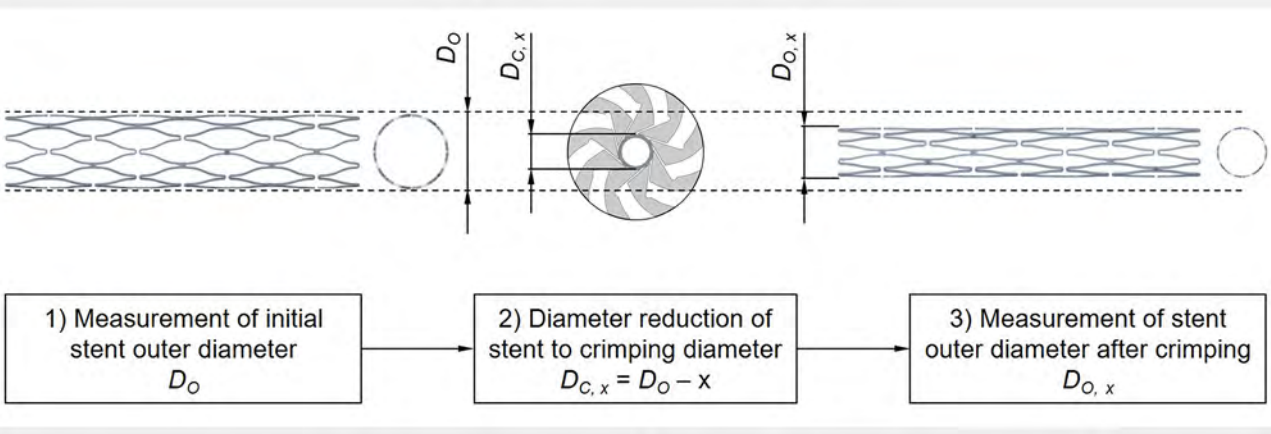


▶ **Fig. 2** Procedure for analysis of crimping and expansion behavior of stents: 1) measurement of initial stent outer diameter at five positions along the longitudinal axis, 2) diameter reduction to a specific crimping diameter, 3) release of stent as well as measurement of stent outer diameter after crimping.

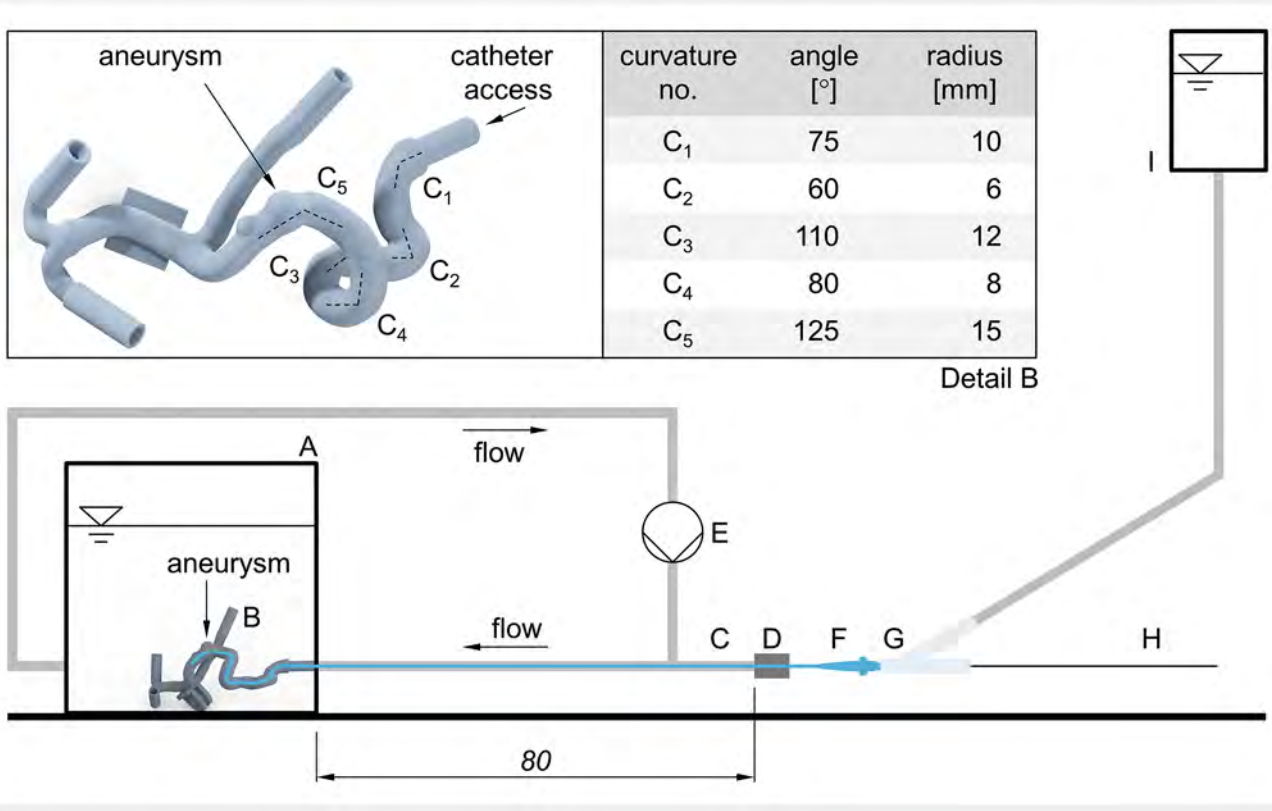


▶ **Fig. 3** Schematic representation of the simulated use test setup: water bath (**A**) including the patient-specific vessel model of the left intradural vertebral artery (**B**) connected to an 80 cm long arterial access vessel (**C**) and a 6F introducer sheath (**D**); Medium circulation via pulsatile pump (**E**); Stent implantation was conducted using an angiography catheter (**F**) and a guide wire (**H**) as pusher wire; Continuous saline flushing (**I**) was implemented using a Tuohy-Borst adapter (**G**). The highly complex curves along the path to the aneurysm are illustrated in Detail B and are quantified by angles and radii.

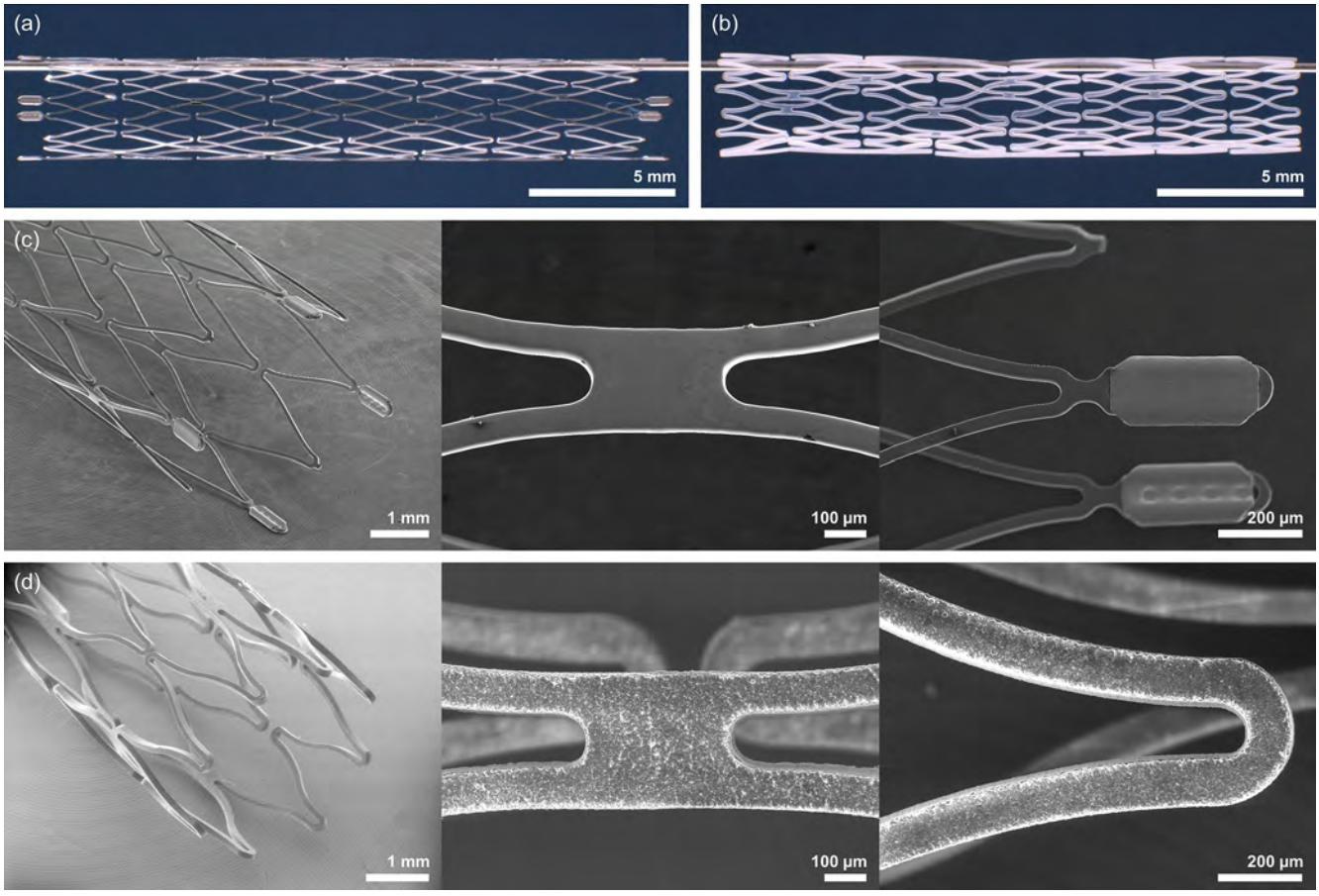


▶ **Fig. 4** Macrographs and SEM images of the Neuroform EZ stent (**a, c**) as well as a representative NBRS prototype (**b, d**); The SEM images show a stent ending (left), a detailed image of the connector (middle), and a detailed image of the end segment (right).

graphy catheter with an inner diameter of 0.038”/1.03 mm (Terumo Radifocus Optitorque, Terumo, Japan) with continuous saline flush through the side port of a Tuohy-Borst adapter (Rotating Hemostatic Valve 0.115”/2.92 mm, Abbot, USA). The catheter tip was positioned distal to the aneurysm neck, using a fitting hydrophilic guidewire (Radifocus Guide wire M, J-tip, Terumo, Japan). After crimping, the NBRS was transferred manually into a straight 4F diagnostic catheter with an inner diameter of 0.038”/1.02 mm (Merit Impress, Merit Medical Systems, USA), serving as the loading device. The loading device tip was inserted into the Tuohy-Borst adapter and secured in the distal catheter hub. The NBRS was transferred into the distal catheter using a fitting straight hydrophilic guidewire (Radifocus Guide wire M, Terumo, Japan) as the pusher wire, and continuously advanced to the distal catheter tip. NBRS expansion was performed by keeping the pusher wire in position and pulling back the catheter and placing it over the aneurysm neck.

### *In vitro* coiling procedure

*In vitro* stent-assisted coiling was performed using a transparent technical vessel model with a parent vessel diameter of 3 mm and a broad-based aneurysm of 4 mm. The expanded Neuroform EZ stent and an NBRS prototype were subsequently inserted into the two-piece acrylic glass aneurysm model which was secured using four plastic screws. The coiling procedure was performed using a guide wire (Transend 0.010", Boston Scientific, USA), a microcatheter (Excelsior SL-10, Stryker, USA) with a steam-shaped tip (60°) and a coil (Target XL 360 Soft 3 mm × 9 cm, Stryker, USA) under combined fluoroscopic (Philips Azurion ClarityIQ, Philips Healthcare, Netherlands) and video guidance (EOS R5, Canon, Japan). Documentation and analysis of the vessel lumen size reduction were carried out by single shot radiographs and macrographs.

## Results

### Manufacturing, geometrical and morphological examination of stents

PLLA tubes with inner and outer diameters of $D_M = 4.00 \pm 0.00$ mm and $D_T = 4.20 \pm 0.01$ mm and a resulting wall thickness of $T_W = 100 \pm 5$ µm were manufactured ($n = 20$). A representative NBRS prototype and the Neuroform EZ stent are shown in ▶ **Fig. 4** as macrographs and SEM images in the expanded state. Both stents show sharp cutting edges and a cylindrical shape without fractures or irregularities. The surface of the electropolished Neuroform EZ stent appeared clearly smoother compared to the NBRS.

▶ **Table 1** Measured dimensions of NBRS prototypes ($n = 3$) and the Neuroform EZ stent ($n = 1$) in fully expanded state as well as measured lengths depending on stent diameter; mean value ± standard deviation of $n = 5$ single measurements per dimension.

| Dimension | Neuroform EZ | | NBRS | |
|---|---|---|---|---|
| Strut thickness $T_S$ [µm] | 70.58 | ± 0.7 | 94 | ± 5.44 |
| Strut width $W_S$ [µm] | 51 | ± 2 | 109 | ± 12 |
| Cell-to-cell length $L_{CTC}$ [µm] | 4791 | ± 29 | 4656 | ± 35 |
| Cell-to-cell height $H_{CTC}$ [µm] | 1278 | ± 9 | 1200 | ± 44 |
| Connector length $L_C$ [µm] | 293 | ± 3 | 358 | ± 8 |
| Connector height $H_C$ [µm] | 222 | ± 7 | 357 | ± 9 |
| Cell opening radius $R_{CO}$ [µm] | 68 | ± 1 | 50 | ± 2 |
| Peak-to-peak cell spacing $L_{CS}$ [µm] | 158 | ± 22 | 103 | ± 24 |
| Outer stent diameter $D_O$ (fully expanded) [mm] | 4.02 | ± 0.07 | 3.89 | ± 0.07 |
| Outer stent diameter $D_{O,C}$ (after crimping) [mm] | 3.95 | ± 0.07 | 3.33 | ± 0.04 |
| Stent length $L_S$ (fully expanded) [mm]* | 20.36 | | 19.79 | ± 0.13 |
| Stent length at $D_O = 3$ mm (vessel) [mm]* | 20.65 | | 20.51 | ± 0.04 |
| Stent length at $D_O = 1.2$ mm (crimped) [mm]* | 20.86 | | 20.66 | ± 0.06 |
| Stent length change (crimped to vessel) [mm]* | 0.21 | | 0.14 | ± 0.04 |
| Stent length change (crimped to vessel) [%]* | 1.01 | | 0.70 | ± 0.21 |

*Stent length for Neuroform EZ measured without radiopaque markers

The results of the geometrical examination of stents are summarized in ▶ **Table 1**. Stent lengths of the Neuroform EZ stent and the NBRS were comparable in the crimped state as well as in the case of the indicated use diameter of 3.0 mm resulting in a similar low length change for both stent types (1 % for Neuroform EZ and 0.7 % for NBRS). The vessel coverage ratio was 43.53 % for the Neuroform EZ stent and 69.19 % for the NBRS due to the larger strut width.

## Radial force and radial stiffness

Exemplary radial force curves are shown in ▶ **Fig. 5**. Radial force increases with decreasing stent diameter for both stent types. For small diameters below 1.2 mm, the NBRS shows an increasing radial force which is attributed to the self-contacting stent struts and does not represent a realistic radial force of the NBRS. RRF and COF at the indicated vessel diameter of 3.0 mm were 1.13 ± 0.22 N and 1.05 ± 0.17 N for the Neuroform EZ stent as well as 0.95 ± 0.09 N and 0.61 ± 0.03 N for the NBRS. The Neuroform EZ stent showed a higher radial stiffness (5.23 ± 0.24 kPa/mm) compared with the NBRS (3.99 kPa/mm) (see also ▶ **Table 2**). After radial force testing (equivalent to crimping down to $D_C = 1.0$ mm and subsequent release), the mean stent diameters $D_{O,C}$ were 3.95 ± 0.07 mm ($n = 1$) for the Neuroform EZ stent and 3.33 ± 0.04 mm ($n = 1$) for the NBRS.

## Kink behavior

▶ **Fig. 6** shows exemplary images of the bent NBRS and Neuroform EZ stent at different bending radii. Both stent structures withstand the deformations and follow the respective radius. The entire stent structure is in contact with the mandrel and no protruding struts were observed on their inner and outer radii. Self-contact of both stent structures was observed for radii smaller than 12.5 mm. No stent kinked at the minimum radius of 2.5 mm.

## Resistance to local deformation

The analyzed Neuroform EZ stent ($n = 1$) and NBRS ($n = 3$) show a comparable deformation behavior under local deformation of $C_{LOC} = 25$ % based on the initial diameter. Respective forces increased to 24 ± 5 mN (Neuroform EZ) and 8 ± 2 mN (NBRS) ($n = 3$ single measurements per stent).

## Simulated use and microstent release *in vitro*

Consecutively, two NBRSs were loaded into the catheter, were advanced through a patient-specific vessel model, and were deployed into the proximity of the aneurysm neck (▶ **Fig. 7**). Microstent delivery could be performed without kinking, buckling, or stent relocation. The stents expanded uniformly and adapted well to the rigid vessel wall.

## *In vitro* coiling procedure

▶ **Fig. 8** shows the documented results of the coiling procedure for both stents. The microcatheter was inserted through the stent struts into the aneurysm model. The coil was released stepwise into the aneurysm sack. Reaching an appropriate coil package density was verified by X-ray. The Neuroform EZ stent as well as the NBRS show only slight deformations within the coiling region, indicating for the ability to retain the coil package.

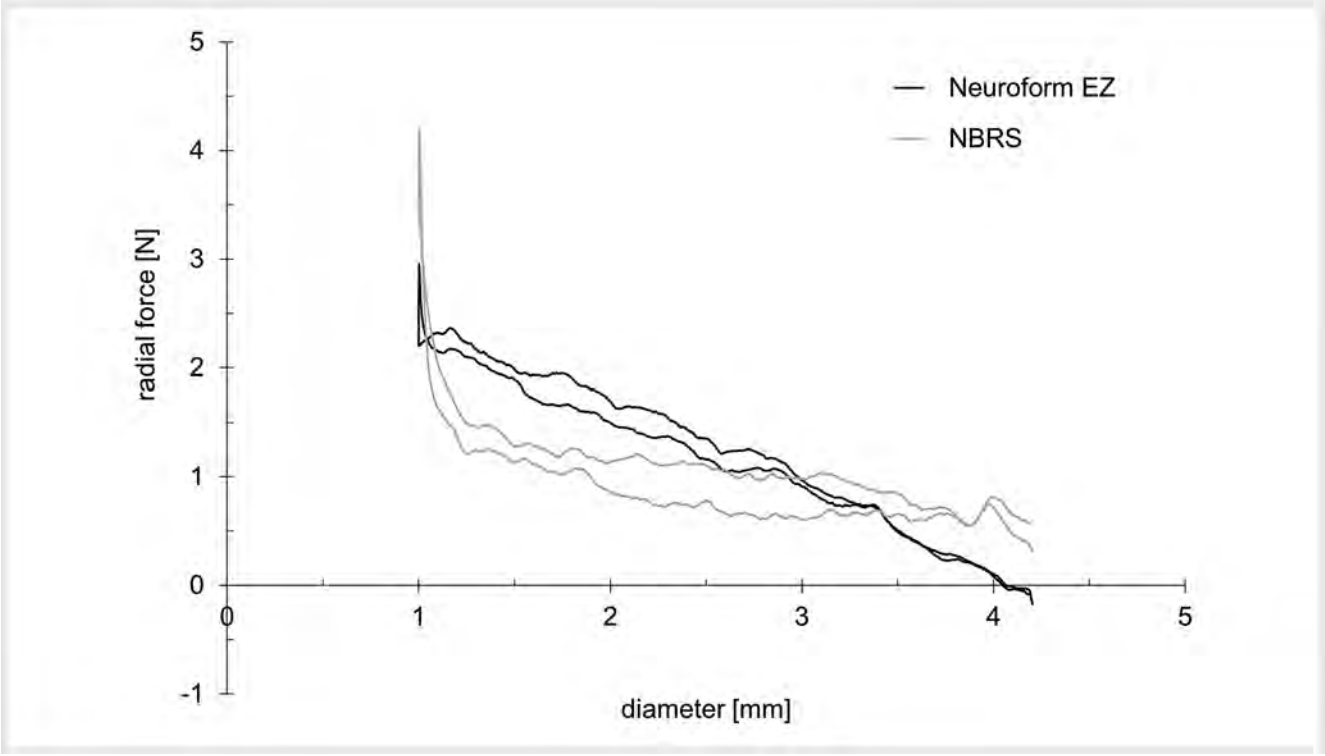


▶ **Fig. 5** Representative radial force curve progression for the Neuroform EZ stent and NBRS during diameter reduction and expansion.

▶ **Table 2** Measured stent properties of NBRS prototypes ($n = 3$) and the Neuroform EZ stent ($n = 1$).

| Measurements | Neuroform EZ ($n = 1$) | | NBRS ($n = 3$) | |
|---|---|---|---|---|
| Radial stiffness [kPa/mm]* | 5.23 | ± 0.24 | 3.99 | ± 0.51 |
| Radial resistive force [N] (at $D_O = 3$ mm)* | 1.13 | ± 0.22 | 0.95 | ± 0.09 |
| Chronic outward force [N] (at $D_O = 3$ mm)* | 1.05 | ± 0.17 | 0.61 | ± 0.03 |
| Force at local deformation (25 %) [mN]* | 22.46 | ± 5.82 | 7.78 | ± 1.54 |
| Stent mass [mg]** | 12.71 | | 5.20 | ± 0.03 |
| Vessel coverage ratio [%]*** | 43.53 | | 69.16 | |

*Mean value ± standard deviation of $n = 8$ single measurements per stent
**Mean value ± standard deviation of $n = 3$ single measurements per stent
***Based on mean values for NBRS prototypes ($n = 8$)

## Discussion

The present study describes the design adaptation, manufacturing, and investigation of a NBRS prototype in comparison to the commercially available Neuroform EZ stent. To compensate for the inferior mechanical properties of PLLA, the NBRS design was adapted with regard to wall thickness and larger connector elements. We investigated the mechanical behavior including radial force, radial stiffness, and resistance against local deformation as well as kinking. In addition, *in vitro* performance tests including a release procedure within a patient-specific vessel model and an *in vitro* coiling procedure were performed.

Femtosecond laser parameter set led to true-to-shape contouring of the semi-finished products with a small heat-affected zone and material re-deposition, thus achieving comparably good results in morphological and geometrical examinations to the Neuroform EZ stent [19]. In general, adequately equal quality of the produced prototypes was determined (e. g., free length between two cells 4656 ± 35 µm for NBRS and 4791 ± 29 µm for Neuroform EZ).

Good crimping capacity of the NBRS prototypes resulted in a minimum outer diameter of 1.0 mm, allowing the use of small catheter profiles.

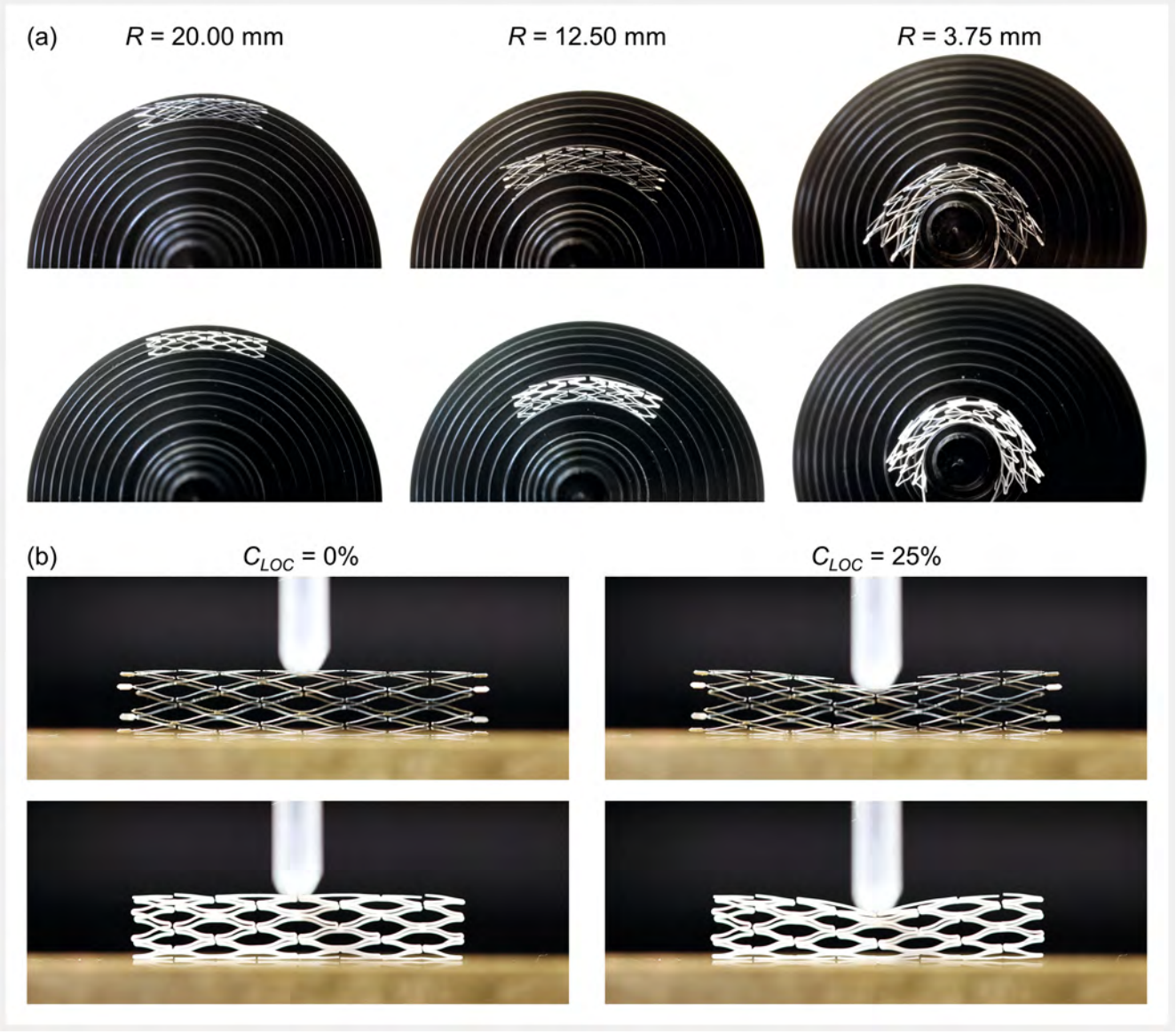


▶ **Fig. 6** Representative macrographs documenting the kink behavior of the examined stents for different radii *R* (**a**) and the behavior of these stents during local compression $C_{LOC}$ (**b**) for the Neuroform EZ stent (top) and NBRS (bottom).

NBRS with a device diameter of 4.0 mm could potentially be used in target vessels with a diameter of less than or equal to 3.0 mm, as the NBRS showed a potential for self-expansion to 3.3 mm.

The radial force of the stent plays a key role regarding fixation inside the target vessel and for supporting the coil package. Cho et al. analyzed the radial force of four commercially available self-expanding stents for neuroradiological applications and found radial force values ranging from 0.47 N to 2.59 N (e. g., 1.07 N to 1.51 N for Neuroform EZ 4.0/20 mm) when reducing its initial diameter to half [4]. Measured radial forces at an indicated use diameter of 3.0 mm for the Neuroform EZ (1.05–1.12 N) were in good agreement to the results of Cho et al. The radial force of the NBRS (0.61–0.95 N) was inferior but in the lower range compared to the results of Cho et al. [4]. Radial stiffness as well as the reaction force after local deformation was lower for the NBRS compared with the Neuroform EZ. However, within the *in vitro* coiling procedure both the Neuroform EZ and NBRS could successfully retain a coil package. Further tests are needed to prove that radial forces are sufficient for a successful *in vivo* application.

Stent flexibility is important to access the commonly tortuous cerebral target vessels. In addition, stent apposition was observed as a key factor for neointimal coverage [20]. Also, incomplete apposition is highly prevalent in patients with very late stent thrombosis (> 30 days) after drug-eluting stent implantation, which can lead to abrupt vascular closure and subsequently to adverse events [21]. Kink behavior results are promising as NBRS adaption to small radii was found, which is generally favorable for use in intracranial vessels.

Patient-specific medical therapy procedures in the digital and analog space are currently a main topic in medical research. Reconstructed 3D models of patient anatomies have great potential

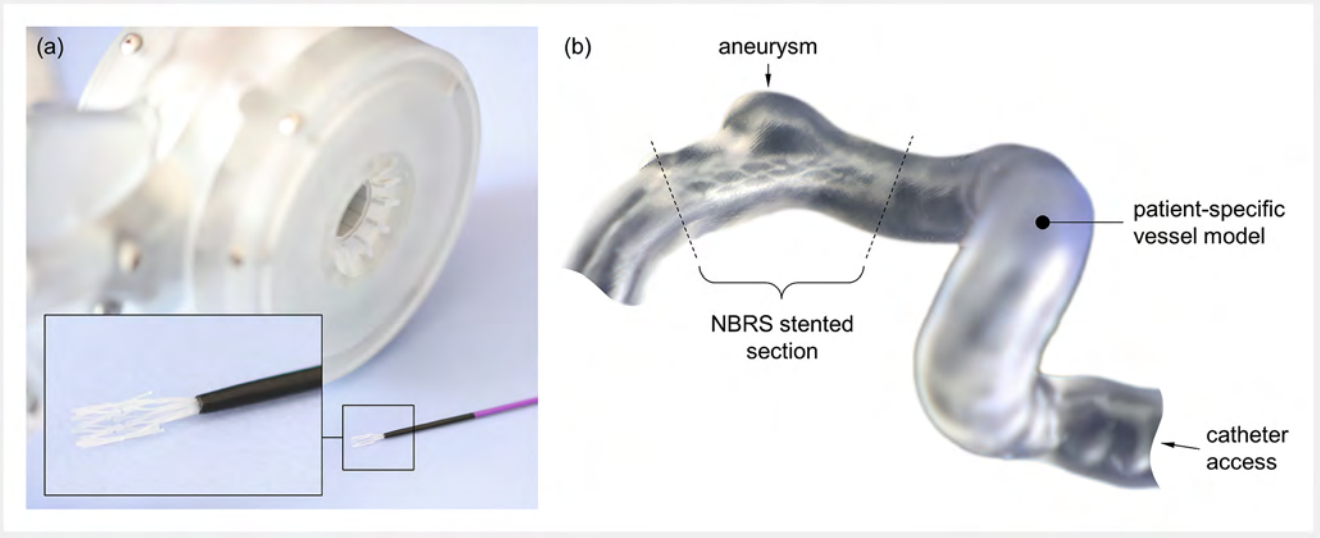


▶ **Fig. 7** Crimping tool and partially loaded NBRS in 4F 0.038“ Merit Impress diagnostic angiography catheter (**a**). Implanted NBRS prototype in 3D-printed patient-specific vessel model of a vertebral artery with an aneurysm (**b**).

for example to assist the education and training of medical professionals as well as to improve implant and device development [17]. Current 3 D printing materials for the model prototypes represent patient-related vessel physiology only to a limited extent. However, it was possible to perform implantation procedures realistically and reproducibly.

To our knowledge, the current article is the first study using a self-expanding bioresorbable polymeric microstent for stent-assisted coiling. Only one report about poly-tyrosine-derived polycarbonate as bulk material in a balloon-expandable stent was found [22]. PLLA degrades completely in one to three years within the human body and can be generally considered as non-toxic and non-inflammatory [23]. However, at an advanced stage of scaffold resorption, very late scaffold thrombosis may occur [24]. Possible implications concerning endothelial damage and potential in-stent restenosis at a late stage were reported, implying that PLLA degradation products have unfavorable side effects on endothelial function [25].

The current study has several limitations: The small number of test samples does not allow for statistical evidence of the test results. Furthermore, only *in vitro* tests were performed to characterize the acute performance properties of the NBRS. However, an *in vivo* test will be needed to guarantee the safety and efficacy of the NBRS.

Future studies should concentrate on optimization of the NBRS stent design, especially the reduction of the strut thickness while maintaining radial force properties and resistance to local deformations. Stent designs should be verified with the help of Finite Element Analysis. To guarantee X-ray visibility, it will be crucial to develop specific X-ray markers to be added to the NBRS stent design.

Future studies should also cover the investigation of fatigue behavior considering relevant load cases such as radial and torsional loading, as well as trackability testing [26, 27].

## Conclusion

This study reported on the design development, manufacturing, and *in vitro* investigation of NBRS prototypes. The NBRS contains a comparable kink behavior to the Neuroform EZ. Vessel lumen size reduction due to kinking of the NBRS is not expected. Radial force, radial stiffness, as well as resistance to local deformation was inferior for the polymeric NBRS. However, as proof of concept, a successful NBRS implantation into a complex patient-specific vessel model as well as stent-assisted coiling in a technical vessel model were conducted. The promising results of this study support the idea of fully bioresorbable microstents for intracranial aneurysm treatment.

## Clinical relevance of the study

The presented *in vitro* measurements characterize an established microstent in comparison to the new bioresorbable microstent for stent-assisted coiling in neurovascular application. The data are suitable to enhance the knowledge and understanding of performance characteristics of the described devices. After further optimization of the bioresorbable stent, there is great potential for the restoration of a natural vessel architecture in patients with intracranial aneurysms.

### Funding

This work was partially funded by the Federal Ministry of Education and Research (BMBF) within the project RESPONSE “Partnership for Innovation in Implant Technology”. Partial funding of the Rostock University Medical Centre within the research funding program FORUN is gratefully acknowledged.

### Conflict of Interest

The authors declare that they have no conflict of interest.

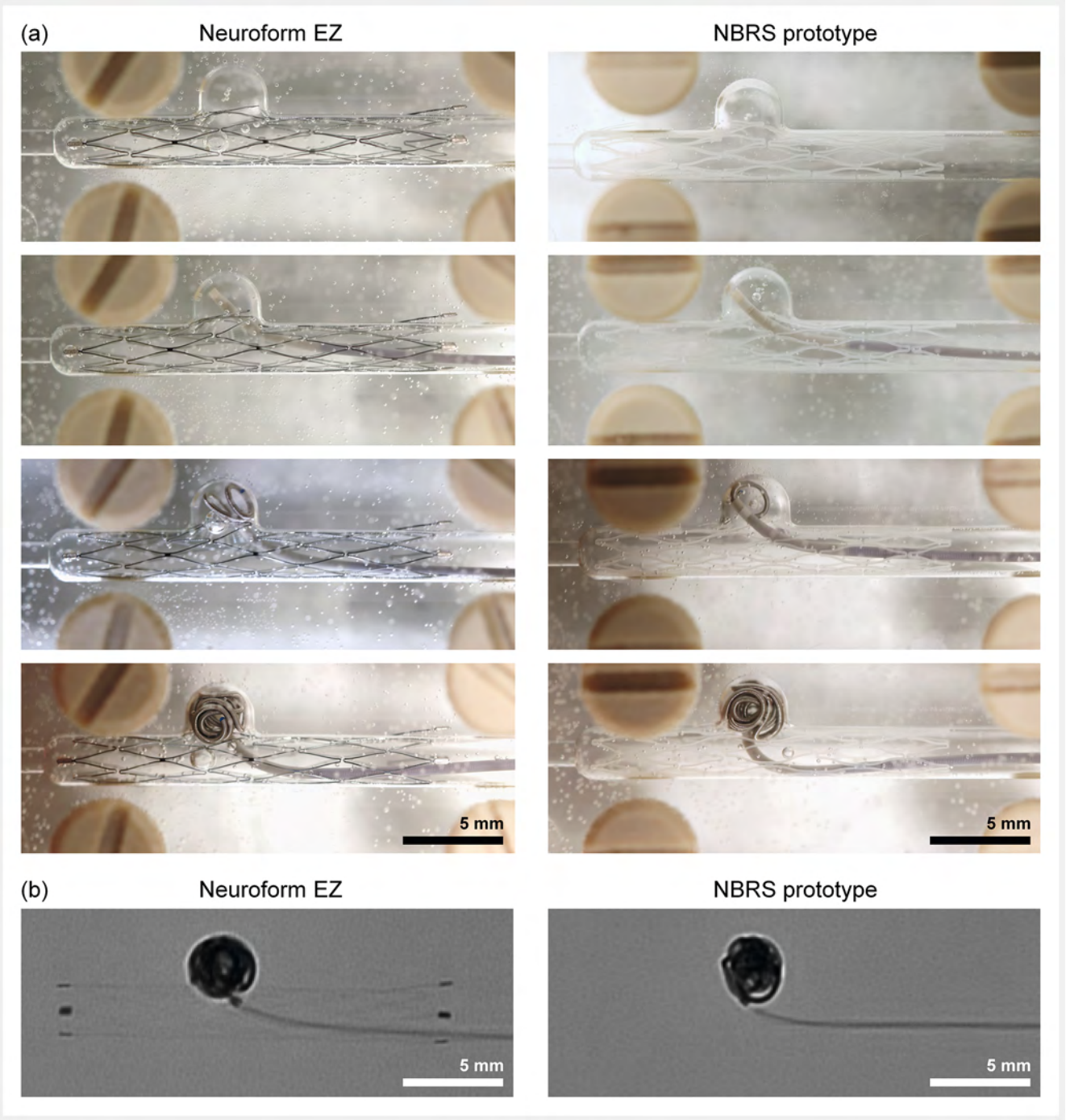


▶ **Fig. 8** Representative macrographs documenting the coiling procedure in a transparent technical vessel model for the examined stents (**a**) and radiographs of the completed procedure of both stents (**b**).

## References

[1] Henkes H, Bose A, Felber S et al. Endovascular Coil Occlusion of Intracranial Aneurysms Assisted by a Novel Self-Expandable Nitinol Microstent (Neuroform). Interv Neuroradiol 2002; 8: 107–119. doi:10.1177/159101990200800202

[2] Wan J, Gu W, Zhang X et al. Endovascular coil embolization of aneurysm neck for the treatment of ruptured intracranial aneurysm with bleb formation. Med Sci Monit 2014; 12: 31–39. doi:10.5469/neuroint.2017.12.1.31

[3] Cai Z-Q, Chai S-H, Wei X-L et al. Comparison of postsurgical clinical sequences between completely embolized and incompletely embolized patients with wide nicked intracranial aneurysms treated with stent assisted coil embolization technique. Medicine (Baltimore) 2018; 97: e10987. doi:10.1097/MD.0000000000010987

[4] Cho S, Jo W, Jo Y et al. Bench-top Comparison of Physical Properties of 4 Commercially-Available Self-Expanding Intracranial Stents. Korean J Intern Med 2017; 12: 31–39. doi:10.5469/neuroint.2017.12.1.31

[5] Mangubat EZ, Johnson AK, Keigher KM et al. Initial Experience with Neuroform EZ in the Treatment of Wide-neck Cerebral Aneurysms. Korean J Intern Med 2012; 7: 34–39. doi:10.5469/neurointern.2012.7.1.34

[6] Yoon NK, Awad AW, Yashar M et al. Stent technology in ischemic stroke. Neurosurg Focus 2017; 42: E11. doi:10.3171/2017.1.FOCUS16507

[7] Li M, Jiang M, Gao Y et al. Current status and outlook of biodegradable metals in neuroscience and their potential applications as cerebral vascular stent materials. Bioact Mater 2022; 11: 140–153. doi:10.1016/j.bioactmat.2021.09.025

[8] Liu Y, Zheng Y, Chen X et al. Fundamental Theory of Biodegradable Metals – Definition, Criteria, and Design. Adv Funct Mater 2019; 29: 1805402. doi:10.1002/adfm.201805402

[9] Grüter BE, Täschler D, Strange F et al. Testing bioresorbable stent feasibility in a rat aneurysm model. J Neurointerv Surg 2019; 11: 1050–1054. doi:10.1136/neurintsurg-2018-014697

[10] Indolfi C, Mongiardo A, Spaccarotella C et al. Neointimal Proliferation Is Associated With Clinical Restenosis 2 Years After Fully Bioresorbable Vascular Scaffold Implantation. Circ Cardiovasc Imaging 2014; 7: 755–757. doi:10.1161/CIRCIMAGING.114.001727

[11] von Zur MühlenC, Reiss S, Krafft AJ et al. Coronary magnetic resonance imaging after routine implantation of bioresorbable vascular scaffolds allows non-invasive evaluation of vascular patency. PLoS One 2018; 13: e0191413. doi:10.1371/journal.pone.0191413

[12] Siewert S, Falke K, Luderer F et al. Development of a biodegradable flow resisting polymer membrane for a novel glaucoma microstent. Biomed Microdevices 2017; 19: 78. doi:10.1007/s10544-017-0218-8

[13] ISO 25539-2:2020, Cardiovascular implants – Endovascular devices – Part 2: Vascular stents, 2020.

[14] Kuang T, Chen F, Chang L et al. Facile preparation of open-cellular porous poly (l-lactic acid) scaffold by supercritical carbon dioxide foaming for potential tissue engineering applications. J Chem Eng 2017; 307: 1017–1025. doi:10.1016/j.cej.2016.09.023

[15] Conti M, De Beule M, Mortier P et al. Nitinol Embolic Protection Filters: Design Investigation by Finite Element Analysis. J Mater Eng Perform 2009; 18: 787–792. doi:10.1007/s11665-009-9408-8

[16] Brandt-Wunderlich C, Schwerdt C, Behrens P et al. A method to determine the kink resistance of stents and stent delivery systems according to international standards. Curr Dir Biomed Eng 2016; 2: 289–292. doi:10.1515/cdbme-2016-0064

[17] Cantré D, Langner S, Kaule S et al. Three-dimensional imaging and three-dimensional printing for plastic preparation of medical interventions. Radiologe 2020; 60: 70–79. doi:10.1007/s00117-020-00739-6

[18] Kemmling A (Hrsg.) FLOWMODDA Flow Models for Device Deployment Tests in Aneurysms. Lübeck: Institut für Neuroradiologie UKSH Lübeck; 2016: 1–9

[19] Huang H, Zheng HY, Lim GC. Femtosecond laser machining characteristics of Nitinol. Appl Surf Sci 2004; 228: 201–206. doi:10.1016/j.apsusc.2004.01.018

[20] Foin N, Gutiérrez-Chico JL, Nakatani S et al. Incomplete stent apposition causes high shear flow disturbances and delay in neointimal coverage as a function of strut to wall detachment distance: implications for the management of incomplete stent apposition. Circ Cardiovasc Interv 2014; 7: 180–189. doi:10.1161/CIRCINTERVENTIONS.113.000

[21] Kuchulakanti PK, Chu WW, Torguson R et al. Correlates and Long-Term Outcomes of Angiographically Proven Stent Thrombosis With Sirolimus- and Paclitaxel-Eluting Stents. Circulation 2006; 113: 1108–1113. doi:10.1161/CIRCULATIONAHA.105.600155

[22] Cockerill I, See CW, Young ML et al. Designing Better Cardiovascular Stent Materials – A Learning Curve. Adv Funct Mater 2020; 31: 2005361. doi:10.1002/adfm.202005361

[23] Ormiston JA, Serruys PW, Regar E et al. A bioabsorbable everolimus-eluting coronary stent system for patients with single de-novo coronary artery lesions (ABSORB): a prospective open-label trial. Lancet 2008; 371: 899–907. doi:10.1016/S0140-6736(08)60415-8

[24] Räber L, Brugaletta S, Yamaji K et al. Very late scaffold thrombosis: intracoronary imaging and histopathological and spectroscopic findings. J Am Coll Cardiol 2015; 66: 1901–1914. doi:10.1016/j.jacc.2015.08.853

[25] Zhengjun H, Wenhua Y et al. Lactic acid-mediated endothelial to mesenchymal transition through TGF-β1 contributes to in-stent stenosis in poly-L-lactic acid stent. Int J Biol Macromol 2020; 155: 1589–1598. doi:10.1016/j.ijbiomac.2019.11.136

[26] Schmidt W, Behrens P, Brandt-Wunderlich C et al. In vitro performance investigation of bioresorbable scaffolds – standard tests for vascular stents and beyond. Cardiovasc Revasc Med 2016; 17: 375–383. doi:10.1016/j.carrev.2016.05.001

[27] Schmidt W, Wissgott C, Andresen R et al. Performance characteristics of modern self-expanding nitinol stents indicated for SFA. Fortschr Röntgenstr 2011; 183: 818–825. doi:10.1055/s-0031-1273445